2015

In vivo MRI signatures of hippocampal subfield pathology in intractable epilepsy.

Maged Goubran

Boris C Bernhardt

Diego Cantor-Rivera

Jonathan C Lau

Charlotte Blinston

See next page for additional authors

IN VIVO MRI SIGNATURES OF HIPPOCAMPAL SUBFIELD PATHOLOGY IN INTRACTABLE EPILEPSY

Maged Goubran [1,2,*], Boris C. Bernhardt [6], Diego Cantor-Rivera [1,2], Jonathan C. Lau [3], Charlotte Blinston [1,2], Robert R. Hammond [4], Sandrine de Ribaupierre [2,3,5], Jorge G. Burneo [3], Seyed Mirsattari [3], David A. Steven [3], Andrew G. Parrent [3], Andrea Bernasconi [6], Neda Bernasconi [6], Terry M. Peters [1,2,5], Ali R. Khan [5,7]

[1] Imaging Research Laboratories, Robarts Research Institute, London, Ontario, Canada

[2] Biomedical Engineering Graduate Program, Western University, London, Ontario, Canada

[3] Epilepsy Program, Department of Clinical Neurological Sciences, Western University, London, Ontario, Canada

[4] Department of Pathology, Division of Neuropathology, London, Ontario, Canada

[5] Department of Medical Biophysics, Western University, London, Ontario, Canada

[7] Department of Medical Imaging, Western University, London, Ontario, Canada

[6] Neuroimaging of Epilepsy Laboratory, McConnell Brain Imaging Center, Montreal Neurological Institute, McGill University, Montreal, Quebec, Canada

* **Corresponding author**

Maged Goubran

mgoubran@stanford.edu

(650) 272-9210

P.O Box 5015 1151 Richmond St. North, London,

Ontario, Canada, N6A 5B7

Running Title

Subfield-specific MRI signatures of HS

Abstract

Our aim is to assess the subfield-specific histopathological correlates of hippocampal volume and intensity changes (T1, T2) as well as diffusion MRI markers in TLE, and investigate the efficacy of quantitative MRI measures in predicting histopathology *in vivo.* We correlated *in vivo* volumetry, T2 signal, quantitative T1 mapping, as well as diffusion MRI parameters with histological features of hippocampal sclerosis in a subfield-specific manner. We made use of on an advanced co-registration pipeline that provided a seamless integration of preoperative 3T MRI with post-operative histopathological data, on which metrics of cell loss and gliosis were quantitatively assessed in CA1, CA2/3, and CA4/DG. MRI volumes across all subfields were positively correlated with neuronal density and size. Higher T2 intensity related to increased GFAP fraction in CA1, while quantitative T1 and diffusion MRI parameters showed negative correlations with neuronal density and/or size in CA4/DG/. Subfield-based multiple linear regression analysis revealed that *in vivo* multi-parametric MRI can predict neuronal loss in all subfields with up to 97% accuracy. Our results, based on an accurate co-registration pipeline and a subfield-specific analysis of MRI and histology, demonstrate the potential of MRI volumetry, diffusion, and quantitative T1 as accurate *in vivo* biomarkers of hippocampal subfield pathology.

Keywords

Hippocampal Sclerosis, Hippocampal Subfields, Histology, MRI, Temporal Lobe Epilepsy

Introduction

Temporal lobe epilepsy (TLE) is the most common form of drug-resistant epilepsy in adults [1]. Hippocampal sclerosis (HS) is the histopathological hallmark of TLE and the most common underlying etiology [2]. It is characterized by cell loss and gliosis in the hippocampal formation, with substantial individual variability in the extent and spatial distribution of these changes. Since early pathological descriptions [3], it has been widely accepted that subfields such as Cornu Ammonis (CA) 1, CA3, CA4, and the dentate gyrus present with marked changes, while CA2 is relatively spared [4]. Across patients, HS encompasses a broad spectrum of structural changes, which can be categorized into different subtypes based on neuropathological grading systems [5-7]. Previous findings have suggested an association between histopathological subtypes, postsurgical seizure outcomes, and postoperative memory impairment [6-9]. In-vivo prediction of distinct subfield atrophy may lead to more accurate TLE diagnosis and improved patient management. It may also play an important role in the early detection and treatment of other neurological and neurodegenerative diseases, such as Alzheimer's disease (West, 2004)**,** stress (McEwen, 1997) or schizophrenia (Harrison, 2004), where the subfields are selectively affected.

MRI has played a key role in the pre-surgical evaluation of TLE, with *in-vivo* volumetry and T2-MRI showing a high utility in identifying HS [10-20]. Landmark studies have shown that global hippocampal atrophy correlates with pathological grades of hippocampal cell loss [10]; and that T2 signal mainly relates to glial cell count, particularly in the dentate gyrus [19]. While these studies represent important steps towards a histopathological validation of MRI markers of HS, assessments have been carried out either on the whole hippocampus or have been restricted to

single subfields. Moreover, comparisons between the resected tissue and MRI did not employ rigorous data co-registration that would allow for a regionally specific correlation between *in-vivo* MRI and histological features. Finally, although previous reports have suggested that diffusion assessments may be a sensitive marker of HS-related changes [21], the exact histopathological correlate of abnormal diffusion in TLE has not been established in humans.

The current study aims to assess the subfield-specific histopathological correlates of an ensemble of advanced MRI markers. Specifically, we evaluated hippocampal volume, T2 intensity, quantitative T1 and diffusion MRI markers in TLE, and investigated their efficacy in predicting histopathology *in vivo*. Our analysis framework is built on a unique co-registration pipeline that allows for seamless integration of preoperative high-resolution MRI with post-operative histopathological data, on which metrics of cell loss and gliosis were quantitatively assessed.

Materials and methods

Patients and Samples

The subjects in this study were 15 patients with drug-resistant TLE (7 males and 8 females, age=36±12 years, range=20-59 years), who underwent anterior temporal lobectomy (ATL) with amygdalohippocampectomy surgery at the London Health Sciences Centre. The hippocampal specimens were resected en-bloc by two surgeons at our centre, with minimal use of ultrasonic aspiration. All subjects underwent preoperative 1.5 Tesla clinical MRI (acquiring T1-weighted, T2-weighted, FLAIR, and diffusion-weighted sequences) and neuropsychological testing, as part of their pre-surgical evaluation. Video-scalp EEG telemetry was employed to identify the

epileptogenic zone, with four patients needing subdural electrode placement to better localize their seizures onset zone. In addition to the 1.5 T conventional MRI sequences, subjects underwent a series of scans on a 3.0 T research scanner as described in the *in-vivo* MRI imaging subsection. ***Table 1*** summarizes the clinical and demographic information for our cohort. Fifteen subjects were originally recruited, however two were discarded from the analysis as the hippocampi were fragmented, and there was insufficient tissue to clinically assess HS or perform automated neuron analysis. Informed consent was collected from all participants prior to their recruitment in the study. This project was approved by the office of Research Ethics of Western University.

MRI acquisition

a) *In-vivo acquisition*

All patients underwent *in vivo* imaging on a 3.0 T Discovery MR750 scanner (General Electric, Milwaukee, WI, USA) using a 32 channel head coil. The DESPOT1-HIFI technique [22] was employed for quantitative T1 mapping, whereby two 3D spoiled gradient echo (SPGR) sagittal T1-weighted scans (TR=8.36 ms, TE=3.71 ms, flip angles =4°/18°, matrix=220x220, slice thickness=1 mm, FOV=220x220 mm^2), as well as an additional sagittal inversion-prepared SPGR volume for B1 mapping (TR=6.4 ms, TE=3.1 ms, flip angle=5°, matrix=220x128, slice thickness=1 mm, FOV=220x200 mm^2) were acquired. For T2-weighted MRI, we employed a sagittal balanced steady-state free precession (bSSFP) sequence (TR=4.6 ms, TE=2.3 ms, flip angles=35°, matrix=220x220, slice thickness=1 mm, FOV=220x220 mm^2). T2 intensity values were normalized with respect to mean intensity in a spherical region in the lateral ventricle ipsilateral to the HS for each patient. An axial spin-echo echo-planar imaging (EPI) sequence

was used to obtain diffusion weighted MRI, with a b-value of 1000 s/mm^2 and 41 diffusion directions (TR=1100 ms, TE=63.2 ms, flip angle=90°, matrix=96x96, slice thickness=2.5 mm, FOV=240x240 mm^2).

b) *Ex-vivo specimen acquisition*

In order to validate our *in-vivo* DTI measurements, high-resolution *ex-vivo* DTI was performed on cases where overnight imaging was feasible and not disruptive to the clinical workflow (N=5). Scanning was performed on a 9.4T small bore Varian MR magnet (Varian, Palo Alto, CA, U.S.A) in a millipede birdcage MP30 coil (Agilent, Santa Clara, CA, U.S.A) after overnight fixation in 10% formalin. Each specimen was immersed in a fluorine-based lubricant 'Christo-lube MCG 1046' (Lubrication Technology, Inc) prior to imaging to avoid susceptibility artifacts at the tissue boundaries. Spin-echo diffusion sequences were acquired (TR = 7.6 ms, TE = 3.8 ms, slice thickness = 0.4mm) with an in-plane resolution of 0.1×0.1 mm and FOV of 38×25.6 mm. We also acquired structural images employing a balanced steady-state free precession sequence (TrueFISP, TR = 7.6 ms, TE = 3.8 ms, flip angle = 30◦, resolution = 0.1 mm isotropic, FOV= 38×25.6×19.2 mm) for in-vivo to ex-vivo image registration.

MRI processing

a) *Quantitative T1*

The T1-weighted volumes co-registered to the first image volume of the session using a rigid transformation obtained with FLIRT (FSL 4.1, http://fsl.fmrib.ox.ac.uk). Quantitative T1 maps were reconstructed using the approach described by Deoni et al.[22].

b) *Diffusion MRI*

Non-linear distortions were corrected by deformable registration of the average unweighted volume to the undistorted T1 map using a diffeomorphic registration method [23, 24]. FMRIB's Diffusion Toolbox (FDT) was used for motion and eddy current correction and estimation of the diffusion tensor. In addition, we computed the two diffusion tensor imaging (DTI) parameters; fractional anisotropy (FA) and mean diffusivity (MD), also known as apparent diffusion coefficient (ADC), which are the most commonly used indices in the epilepsy literature, defined as:

$$FA = \frac{\sqrt{3[(\lambda_1 - \langle\lambda\rangle)^2 + (\lambda_2 - \langle\lambda\rangle)^2 + (\lambda_3 - \langle\lambda\rangle)^2}}{\sqrt{2(\lambda_1^2 + \lambda_2^2 + \lambda_3^2)}},$$

where

$$\langle\lambda\rangle = MD = \frac{(\lambda_1 + \lambda_2 + \lambda_3)}{3},$$

$\lambda_1, \lambda_2, \lambda_3$ are the eigenvalues of the diffusion tensor. Using linear registration (FLIRT), we transformed and resampled the resulting diffusion maps to the coordinate system defined by T1 map (1 mm isotropic voxel size).

Quantitative histology

Resected specimens underwent accessioning and gross description by the Department of Pathology at London Health Sciences Centre. The numerous challenges in our quantitative histology pipeline include the high complexity of en-bloc resections, as the difficulty in preserving atrophic hippocampi throughout histological processing, and the tendency for the tissue to deform and occasionally form fissures (partially due to the differential shrinkage of gray and white matter). To better preserve specimen architecture, the samples were bissected in the coronal plane and each half embedded in agar for stabilization and support during processing and sectioning. Each half was sectioned into thick coronal slices (4.4 mm spacing), parallel to the initial cut using a deli slicer. Blocks were then embedded in paraffin and sectioned at a thickness of 8 μm. Hematoxylin and eosin (H&E) stain was applied to slides from each block, in addition to the following immunohistochemical (IHC) stains: neuronal nuclear protein (NeuN) (monoclonal antibody; 1:400; EMD Millipore, Billerica, Massachusetts) as a marker for neuronal nuclei and the perinuclear soma, and GFAP (polyclonal antibody; 1:4000; Dako, Agilent Technologies, Santa Clara, California) as a marker for gliosis. To minimize variability between slides, batch IHC processing was performed on a Dako Autostainer Link 48. Resulting slides were digitized on a ScanScope GL (Aperio Technologies, Vista, CA, USA) bright field slide scanning system at a maximum of 20x optical zoom, and automatically stitched to form full-frame multi-resolution images stored in BigTIFF file format (maximum pixel resolution 0.5 μm).

We quantified NeuN using field fraction estimates (i.e., the proportion of pixels in the field that are positively-stained). These estimates are sensitive to the packing density and cell-size of neuronal cell bodies and processes and have been previously employed to represent neuronal integrity [25-27]. Similarly, we quantified field fraction estimates of GFAP IHC, which is

sensitive to reactive astrogliosis and analyzed the full resolution slides in blocks of 100x100 um using MATLAB (The MathWorks Inc., Natick, MA, USA). To provide local estimates of neuron density and size we developed a method for segmenting cell bodies of pyramidal and granular neurons. This technique first extracts the colour component related to immuno-positive staining using colour deconvolution [28] preceding a watershed-based segmentation procedure [29] for splitting joined or connected neurons, and removes objects smaller than a predefined area defined as noise (less than 14 μm^2). Resulting neuron segmentations provide the neuronal density (number of neurons) per field, as well as the mean area (size) of cell bodies, within the field. To further discriminate between pyramidal neurons of the CA subfields and granular neurons of the dentate gyrus, we used area thresholds (125 and 50 μm^2 respectively). Neuron-specific quantitative features in each field of these images were extracted using a custom algorithm written in MATLAB. Manual counts taken from two randomly selected fields per slice within the CA subfields and the dentate gyrus by one rater (blinded to the automated counts) were employed to validate our automated cell segmentation for pyramidal and granular neuron quantification. Automated (*A*) and manual (*M*) segmentation achieved a high agreement Kappa (κ) = (*A*-*M*) / (1-*M*) = 98% for pyramidal cell counts and κ = 96% for granular cell counts. ***Figure 1*** illustrates this procedure and demonstrates the quantitative histological features: neuronal density (for both CA and DG), mean neuron size, and GFAP field fraction**.** Neuronal density data from the least sclerotic specimens were used as references to compute percent cell loss per subfield for each patient. We generated as well a three-level (1: no HS, 2: moderate, 3: severe) *qualitative* HS subtype classification based on expert clinical assessment that combined radiological and histology reports. The second level definition was based on moderate CA1 atrophy or mild involvement of both CA1 and C4. The third level was based on severe global

atrophy in CA1 and CA3 & 4. No subject presented as atypical CA4-only atrophy in our cohort, either in the histology reports or the quantitative analysis.

Histology feature extraction

A single rater (MG) manually delineated hippocampal subfields on histology slices, downsampled to 20μm pixel size using ITKSNAP [30], and were confirmed by neuropathologist (RH). Our segmentation protocol is based on the Duvernoy hippocampus atlas [31], with the following boundary definitions: The border between the subiculum and CA1 was defined as a horizontal line at the edge of the subiculum extending from the inferior border of the dentate gyrus and the hippocampal sulcus, as shown in the top row of ***Figure 2***. The CA1/CA2 boundary was designated as the point at which a noticeable decrease in width of the CA1 subfield was observed, following the most lateral point of the DG. The CA2/CA3 boundary was defined at the most medial point of the superior curve of the dentate gyrus where a gradient of pyramidal cell density is observed between the subfields. The opening of subfields into the globular region of the hippocampal formation formed the CA3/CA4 border. The remaining globular region of the hippocampal formation was marked as CA4. The dentate gyrus was divided into two labels, one encompassing the granular layer and another combining both molecular and polymorphic layers surrounding the granular cells. ***Figure 2*** shows examples of subfield delineation on histology slices from three patients from our cohort with mild, moderate and severe sclerosis.

MRI parameter extraction

We first applied our previously described MRI to histology [32, 33] registration pipeline, which allowed for the identification of the MRI slice that best corresponded to the cut histology slice

(*Figure 3*). Instead of relying on imaging parameters from segmented subfields along the entire length of the hippocampus**,** parameters can be analyzed from a select target region encompassing the MRI slice corresponding to a given histological slice. For more robust correlations, we modelled uncertainty stemming from registration (approx. 2.5 mm) [32, 33] and histological sectioning errors (variance in sectioning histology slices from the face of blocks, approx. 1 mm) [34]. Specifically, MRI data adjacent to the corresponding slice were cropped and weighted using a sinc function with FWHM=3mm, giving data adjacent to the closest corresponding MRI slice in the sagittal plane a higher weighting than those more distant.

Within a given target region, subfields were then manually segmented by a single rater (MG). This segmentation protocol mirrors that employed on histology and is similar to that described in our previous work at 7.0 T [35]. The MRI protocol was confirmed by consensus with a neurologist (NB) and a neuropathologist (RH). Assessment was restricted to CA1, CA2/3, and CA4/DG. It should be noted that MRI parameter extraction was performed in the intrinsic *in vivo* space (1 mm isotropic) and not the upsampled space to avoid resampling the quantitative maps.

Statistical analysis

Statistical analyses were performed using SPSS statistics (version 20, IBM, Armonk, NY) and JMP statistical software (version 10, SAS, Cary, NC). Prior to analysis, MRI parameters and histological features were internally z-scored. It should be noted that DTI measures were only assessed in CA1 and CA4/DG in the subfield-specific analysis, due to the lower native resolution of the diffusion MRI acquisition. The statistical analysis was stratified into four distinct experiments:

A. MRI-histology correlations

i. *Univariate correlation analysis*

We systematically assessed pair-wise, non-parametric (Spearman Rho) correlations between individual histological parameters relating to neuronal characteristics (neuronal size and density) and putative MRI markers of neuronal loss (subfield volume and T1 intensity [36]). In a second step, we evaluated correlations between histological GFAP field fraction and MRI-derived T2-w intensity. In a more exploratory diffusion-histology assessment, we correlated histological parameters with FA and MD. Multiple comparisons were corrected at a family-wise error (FWE) of $p < 0.05$ using non-parametric permutation tests [37]. Permutation tests were performed in MATLAB based on two-tailed Spearman rank correlations with 100,000 random permutations. The family-wise error corrected *p*-values (alpha=0.05) for each comparison were obtained using the distribution of the most extreme statistic calculated for each permutation.

ii. *Multiple linear regressions.*

To test the efficacy of quantitative, multi-parametric MRI in pre-operatively predicting neuronal loss per subfield, multiple linear regression analyses were performed between a) subfield-specific MRI parameters and percent loss of neurons for each subfield, b) MRI parameters from all subfields and percent neuronal loss for each subfield.

B. Clinical correlations

In addition, we assessed the correlations between each of the above variables and clinical variables such as age of seizure onset, duration of epilepsy and short-term Engel seizure outcome.

C. Validation Experiments

We performed three experiments to validate our *in-vivo* DTI measurements and provide further evidence that our correlation analysis is not driven by single outliers or confounds such as the partial volume effect.

i. *High-resolution ex-vivo DTI*

This experiment was performed with the aim of validating our *in-vivo* DTI measurements with higher resolution *ex-vivo* data. We first employed our registration pipeline to obtain a mapping between *ex-vivo* data and histology then warped the histology labels to the *ex-vivo* space. These labels were then used to initialize the segmentation and to define the *ex-vivo* corresponding slices. Segmentation adjustments were applied by the same rater (if needed post-registration) on T2-weighted structural images, prior to extraction of diffusion parameters from FA and MD maps and comparison with *in-vivo* measurements. Voxels at the gray matter-CSF boundary (in CA1 and CA2) were not segmented to avoid CSF contamination in our validation datasets. Correlation coefficients were computed between both scanning sessions for both diffusion parameters.

ii. *Label Erosion*

In addition, we eroded the subfield segmentation labels inward and repeated all the univariate correlation analysis as a further demonstration that partial volume effects did not influence our results.

iii. *Bootstrapping*

We employed the bootstrapping technique, with a sample size of 1000 and 95% bias corrected confidence intervals on all the tested correlations, to better estimate the confidence intervals of the presented correlation coefficients and ensure the reliability of our results. We will present the results of this experiment alongside the univariate correlation results, where each correlation coefficient is followed by its 95% bias corrected lower and upper confidence intervals from bootstrapping.

Results

A. MRI-histology correlations

*i. Univariate correlations (**Table 2** and **Figure 4**).*

Across all subfields, we observed a consistent positive correlation between MRI-derived subfield volume and histology-derived neuronal density and size, with highest effect sizes in CA1 (density: r_s = 0.910 (0.633, 0.997), p_{fwe} < 0.001, and size: r_s = 0.830 (0.302, 0.994), p_{fwe} < 0.001). Correlations for the other parameters were confined to single subfields. Specifically, MD was negatively correlated with pyramidal cell density within CA4/DG (r_s = -0.833 (-0.479, -0.975), p_{fwe} < 0.001) and T1 negatively correlated with both neuronal markers in the same subfield (size: r_s = -0.830 (-0.497, -0.994), p_{fwe} < 0.001, and density: r_s = -0.781 (-0.320, -0.966), p_{fwe} = 0.006). On the other hand, higher T2-weighted intensity related to increased GFAP fraction in CA1 (r_s = 0.835 (0.518, 0.950), p_{fwe} < 0.001).

ii. *Multiple linear regressions.*

a) *Subfield-specific*

Multiple linear regression analysis demonstrated that multi-parametric MRI can accurately predict subfield neuronal loss. Across all subfields, volume was a consistent feature, and was selected together with T2 in CA1 (adjusted $R^2 = 0.88$, $p < 0.001$), with T1 in CA2/3 (adjusted $R^2 = 0.73$, $p = 0.001$) and second to MD in CA4/DG (adjusted $R^2 = 0.70$, $p = 0.005$).

b) *Cross subfields regressions*

As for MRI parameters from all subfields, CA4/DG volume as well as CA1 T1 and FA, predicted CA1 percent neuronal loss with high accuracy (adjusted $R^2 = 0.90$, $p < 0.001$). Volume and T1 parameters from CA2/3 as well as CA4/DG MD and T2 predicted CA2/3 percent loss with very high accuracy (adjusted $R^2 = 0.96$, $p < 0.001$). Finally, loss in CA4 was predicted with equivalent accuracy using CA4/DG and CA2/3 volume and MD (adjusted $R^2 = 0.97$, $p < 0.001$). ***Table 3*** summarizes the multiple linear regression results for the subfield-specific experiment. The model fit for the prediction of neuronal loss of the four analyzed subfields from subfield-specific parameters is presented in ***Figure 5***.

B. Clinical correlations

In the subfield-specific correlation analysis, only CA2/3 T1 negatively correlated with short-term Engel outcomes with prolonged T1 values relating to better outcomes ($r = -0.701$, $p_{fwe} = 0.012$) and similarly CA4 GFAP field fraction was the only histological feature to correlate with outcomes with increased gliosis in CA4 associating with worse outcomes ($r = 0.695$, $p_{fwe} = 0.012$). Moreover, our qualitative HS subtypes classification (based on clinical MRI and histology reports) correlated with quantitative neuronal density within the three CA subfields (CA1: $r = 0.842$, $p < 0.001$, CA2/3: $r = 0.755$, $p = 0.003$, CA4: $r = 0.920$, $p < 0.001$).

C. Validation experiments

i. *High-resolution ex-vivo DTI*

Figure 6 presents the comparison between *in-vivo* and *ex-vivo* diffusion parameters (FA and MD) for five subjects. The good agreement between the two sessions, in both CA4 as well CA1, provides support for the much larger voxel size present in the *in-vivo* diffusion measurements. CA4 had higher correlations, between *ex-vivo* and *in-vivo* DTI for both MD (r = 0.88) and FA (r = 0.72), than CA1 (MD: r = 0.58, FA= r = 0.52). This could be due to the curved shape of CA1, which compromises gray matter values adjacent to CSF in *in-vivo* imaging. The shift in diffusion measurements, highlighted by the graphs in the figure, between *in-vivo* and *ex-vivo* is probably attributed to fixation and tissue processing effects on the specimens' microstructure. CA2 and 3 were not included in this analysis due to their relatively smaller size compared to our *in-vivo* DTI voxel size.

ii. Label erosion

Findings remained highly significant even when subfield labels were eroded prior to analysis as described earlier, suggesting minimal confounds due to partial volume effect (Suppl. Table 1).

Discussion

This is the first study to investigate the histopathological substrates of volume, T2, quantitative T1 relaxometry while employing high resolution maps at 3.0 T and a comprehensive mapping between MRI and pathology. A number of studies previously correlated T2 and volumetry with pathology in the context of hippocampal sclerosis [10-20]. However, they only focused on whole hippocampus MRI parameters or correlated pathology findings on a histology slice with subfield parameters extracted from the entire hippocampus or employed *in vivo* scans with low out-of-

plane resolution (> 3 mm) and no registration was preformed to establish correspondences between MRI and histology [12-15, 17, 18]. Although previous studies investigated diffusion changes in patients with HS and demonstrated increased MD as well as decreased FA in the ipsilateral hippocampi and white matter [38-42], this is the first to investigate histopathological correlates of diffusion metrics in TLE within the hippocampal subfields. Our registration protocol validates our high-resolution MRI maps with quantitative histology to better understand the pathological substrates of our imaging findings. These features may be more sensitive to neuronal degeneration as distinct from qualitative assessment or quantitative grading of neuronal loss as they provide a continuous measurement of pathologies.

Biological Interpretations

In our correlation analysis, pre-operative subfield volumetry was highly correlated with subfield density (specifically in CA1). Numerous studies have reported that neuronal density within the subfield may directly relate to volume atrophy [10, 11, 13, 19, 20]. The presented subfield-specific correlation analyses confirmed these previous findings.

Mean diffusivity was the most prominent MRI marker, other than volume, for neuronal density. In our subfield-specific analysis, MD was negatively correlated with neuronal density and size of CA4, demonstrating the importance of this MRI parameter in determining subtypes pre-operatively. A previous study analyzing relationships between diffusion maps and cell density in malignant brain tumours described an analogous association between MD and tumour core cell density [43]. The loss of neurons in the hippocampal subfields may lead to less restricted, water diffusion and thus higher diffusivity. A similar interpretation can be described for the

relationship between MD and neuronal size: as neuronal cell bodies shrink, the proportion of intra-neuronal water is reduced thereby increasing diffusivity. Given the limitations of *in-vivo* DTI, we cannot precisely assess the nature of the architectural changes related to MD, but we hope to explore these issues further using high-resolution *ex-vivo* DTI of the resected specimens.

It has been suggested [19] that in-vivo T2 relaxation relates to dentate glial cell count, whereas a more recent study found no correlation between ex-vivo T2-w and GFAP field fraction in the subfields [44]. In our results, T2 also correlated with increased GFAP field fraction expression in CA1, which represents reactive gliosis (astrocytic and microglial proliferation), but failed to show a significant correlation in the dentate gyrus**.** T1 was correlated as well with neuronal size/density in CA4. An analogous relationship between *ex-vivo* GM T1 values and neuronal density has been previously described in patients with multiple sclerosis [45]. Cell loss will likely result in an increase in the extra-cellular space, thus the intra-cellular water will decrease as extra-cellular water increases, which in turn would increase T1 [46]. The presence of a significant association between T1 and neuronal markers in CA4/DG may be due to the high content of zinc in the mossy fiber projections from the dentate gyrus [47]. Our previous study [36], focused on investigating the histopathological correlates of quantitative MRI within the neocortex, demonstrated that in-vivo T1 and FA negatively correlated with density of small caliber neurons. We did not see this relationship for FA in this analysis of the hippocampus, which could be due to the inherent differences in myeloarchitecture and cytoarchitecture that exist between the hippocampus and lateral neocortex. Both studies confirm the power of quantitative T1 mapping and diffusion MRI as *in vivo* biomarkers for hippocampal and

neocortical pathology in TLE, and their potential use to detect pathology in other neurological disorders.

Clinical findings and insights

Multiple linear regression analysis revealed that volume and MD are the most prominent parameters in predicting neuronal loss, with increased accuracy when adding T2. This observation mirrors the correlation analysis where MD and volume were the parameters with the highest number of associations with histological features. T2 was correlated with GFAP field fraction in CA1 whereas MD was correlated with density in CA4, while both have similar insignificant trends in other subfields. A larger cohort may be needed to observe their predictive ability in other subfields. Hippocampal neuronal loss has been previously shown to potentially predict patient outcomes [48] and memory deficits [49]. Predicting subfield loss from *in vivo* quantitative MRI has the potential to non-invasively localize pathology and determine the extent of hippocampal atrophy, with a precision previously unachievable. It may also help classify patients into different HS subtypes and decide on the merit of their surgical candidacy. Moreover, it may help identify select hippocampal subfields for targeting electrodes used for neurostimulation therapy or MRI-guided laser ablation, as an alternative to resective surgical intervention.

The association between the qualitative HS subtype classification and neuronal density within the CA subfields, validates the accuracy of our automated neuron quantification procedure. Some reports have previously shown that hippocampal sclerosis subtypes have different post-operative outcomes [8, 9], and correlate with seizure duration and onset [50]. The Engel

outcomes presented in this study are reported in the short-term follow up with the average time since surgery for our cohort being just under two years (22 months). CA2/3 T1 was the only *in-vivo* MRI parameter to correlate with outcomes in our cohort, which mirrors the classification results demonstrating CA2's ability to represent the spectrum of atrophy across patients.

Limitations and technical considerations

A limitation of this work is the lack of normative control data for histology, and hence in our assessment, the least sclerotic specimens were used as reference for computation of percentage cell loss. We also employed histological measurements from one optimal slide per subject, which may have biased the results. This was due to the restricted size of the resected specimens (only a fraction of the hippocampus is resected at times) and the large variability in specimen sizes, as well as effects of tissue breakage and fragmentations. These limitations, in addition to the need to reserve part of the specimen in tissue banks for clinical use, restricted the analysis to a maximum of one histology slide (for some subjects) where all the CA subfields are clearly visible. In addition, we employed an approximation of T2 values using intensity-normalized T2-weighted images, as some failed T2-weighted acquisitions for an earlier subset of patients prevented us from computing DESPOT2 for all subjects. We opted to manually segment the subfields on MRI, instead of relying on an automated technique, which uses a statistical model with Markov random field priors to delineate subfield boundaries based on T1-weighted MPRAGE MR sequences [20]. Although this approach is more time consuming and possibly prone to rater-bias, it produces more accurate labels specifically in very sclerotic hippocampi, and those with malrotation where the image signal to noise, contrast and resolution, as well as morphology are not sufficient to guide the automated technique. Another way to correlate pre-

operative MRI and pathology is through direct registration of both modalities [32] and warping of regions of interest from histology to *in vivo* space. However, for this technique to be effective, image resolution of pre-operative volumes needs to be sub-millimetric. For example, if *in vivo* maps have a 1 mm isotropic resolution, smaller subfields (i.e. CA2 and CA3) warped from histology would only occupy 2 or 3 voxels on a slice in the in-vivo space, which would challenge the accuracy of the results.

Conclusion

This is the first study to investigate the histopathological substrates of *in vivo* volume, T2, quantitative T1 relaxometry while employing high resolution maps at 3.0 T and a comprehensive mapping between MRI and pathology. It is also the first direct investigation of histopathological correlates of diffusion metrics in TLE within the hippocampal subfields. Moreover, we developed and validated an automated quantitative histology procedure for quantification of neuronal density, size and NeuN and GFAP field fractions. We have demonstrated that volume, MD and T1 are sensitive markers for neuronal integrity in the subfields and confirmed that T2 is a marker of gliosis. Finally, we have shown that *in vivo* multi-parametric MRI can predict subfield neuronal loss in all subfields with very high accuracy. This work suggests that *in vivo* subfield volumetry, diffusion and quantitative MRI have the potential to non-invasively localize pathology and determine the extent of hippocampal subfield atrophy, with increased precision.

Acknowledgments

The authors would like to thank Cathie Crukley, Robert Mayer and Catherine Currie for their assistance and support throughout the study.

This work was supported by the Canadian Institute of Health Research (MOP 184807) and the Canada Foundation for Innovation (20994). MG was supported by the NSERC Create Grant CAMI award at Western University.

References

1. Engel J. A proposed diagnostic scheme for people with epileptic seizures and with epilepsy: report of the ILAE Task Force on Classification and Terminology. Epilepsia. 2001;42(6):796-803.

2. Thom M, Eriksson S, Martinian L, et al. Temporal lobe sclerosis associated with hippocampal sclerosis in temporal lobe epilepsy: neuropathological features. Journal of neuropathology and experimental neurology. 2009;68(8):928-38.

3. Sommer W. Erkrankung des Ammonshorns als aetiologisches Moment der Epilepsie. European Archives of Psychiatry and Clinical Neuroscience. 1880;10(3):631-75.

4. Al Sufiani F, Ang LC. Neuropathology of temporal lobe epilepsy. Epilepsy research and treatment. 2012;2012.

5. Blumcke I, Coras R, Miyata H, Ozkara C. Defining clinico-neuropathological subtypes of mesial temporal lobe epilepsy with hippocampal sclerosis. Brain pathology. 2012 May;22(3):402-11.

6. Blümcke I, Pauli E, Clusmann H, et al. A new clinico-pathological classification system for mesial temporal sclerosis. Acta neuropathologica. 2007;113(3):235-44.

7. Blümcke I, Thom M, Aronica E, et al. International consensus classification of hippocampal sclerosis in temporal lobe epilepsy: a Task Force report from the ILAE Commission on Diagnostic Methods. Epilepsia. 2013;54(7):1315-29.

8. Thom M, Liagkouras I, Elliot KJ, et al. Reliability of patterns of hippocampal sclerosis as predictors of postsurgical outcome. Epilepsia. 2010 Sep;51(9):1801-8.

9. Savitr Sastri BV, Arivazhagan A, Sinha S, et al. Clinico-pathological factors influencing surgical outcome in drug resistant epilepsy secondary to mesial temporal sclerosis. Journal of the neurological sciences. 2014 May 15;340(1-2):183-90.

10. Cascino GD, Jack CR, Parisi JE, et al. Magnetic resonance imaging–based volume studies in temporal lobe epilepsy: pathological correlations. Annals of neurology. 1991;30(1):31-6.

11. Lencz T, McCarthy G, Bronen RA, et al. Quantitative magnetic resonance imaging in temporal lobe epilepsy: relationship to neuropathology and neuropsychological function. Annals of neurology. 1992;31(6):629-37.

12. Jackson G, Connelly A, Duncan J, Grünewald R, Gadian D. Detection of hippocampal pathology in intractable partial epilepsy Increased sensitivity with quantitative magnetic resonance T2 relaxometry. Neurology. 1993;43(9):1793-.

13. Van Paesschen W, Revesz T, Duncan J, King M, Connelly A. Quantitative neuropathology and quantitative magnetic resonance imaging of the hippocampus in temporal lobe epilepsy. Annals of neurology. 1997;42(5):756-66.

14. Coan AC, Kobayashi E, Li LM, Cendes F. Quantification of hippocampal signal intensity in patients with mesial temporal lobe epilepsy. Journal of Neuroimaging. 2003;13(3):228-33.

15. Coan AC, Kubota B, Bergo FP, Campos BM, Cendes F. 3T MRI quantification of hippocampal volume and signal in mesial temporal lobe epilepsy improves detection of hippocampal sclerosis. AJNR American journal of neuroradiology. 2014 Jan;35(1):77-83.

16. Kuzniecky R, Bilir E, Gilliam F, et al. Multimodality MRI in mesial temporal sclerosis: relative sensitivity and specificity. Neurology. 1997;49(3):774-8.

17. Mackay C, Webb J, Eldridge P, Chadwick D, Whitehouse G, Roberts N. Quantitative magnetic resonance imaging in consecutive patients evaluated for surgical treatment of temporal lobe epilepsy. Magnetic resonance imaging. 2000;18(10):1187-99.

18. Goncalves Pereira PM, Oliveira E, Rosado P. Relative localizing value of amygdalo-hippocampal MR biometry in temporal lobe epilepsy. Epilepsy research. 2006 May;69(2):147-64.

19. Briellmann RS, Kalnins RM, Berkovic SF, Jackson GD. Hippocampal pathology in refractory temporal lobe epilepsy T2-weighted signal change reflects dentate gliosis. Neurology. 2002;58(2):265-71.

20. Schoene-Bake JC, Keller SS, Niehusmann P, et al. In vivo mapping of hippocampal subfields in mesial temporal lobe epilepsy: Relation to histopathology. Human brain mapping. 2014 Sep;35(9):4718-28.

21. Wieshmann UC, Symms MR, Barker GJ, Birnie KD, Shorvon SD. Water diffusion in the human hippocampus in epilepsy. Magnetic resonance imaging. 1999;17(1):29-36.

22. Deoni SC. High-resolution T1 mapping of the brain at 3T with driven equilibrium single pulse observation of T1 with high-speed incorporation of RF field inhomogeneities (DESPOT1-HIFI). Journal of magnetic resonance imaging : JMRI. 2007 Oct;26(4):1106-11.

23. Beg MF, Miller MI, Trouvé A, Younes L. Computing large deformation metric mappings via geodesic flows of diffeomorphisms. International journal of computer vision. 2005;61(2):139-57.

24. Huang H, Ceritoglu C, Li X, et al. Correction of B0 susceptibility induced distortion in diffusion-weighted images using large-deformation diffeomorphic metric mapping. Magnetic resonance imaging. 2008;26(9):1294-302.

25. Eriksson SH, Free SL, Thom M, et al. Correlation of quantitative MRI and neuropathology in epilepsy surgical resection specimens--T2 correlates with neuronal tissue in gray matter. Neuroimage. 2007 Aug 1;37(1):48-55.

26. Eriksson SH, Free SL, Thom M, et al. Quantitative grey matter histological measures do not correlate with grey matter probability values from in vivo MRI in the temporal lobe. Journal of neuroscience methods. 2009 Jun 30;181(1):111-8.

27. Lockwood-Estrin G, Thom M, Focke NK, et al. Correlating 3T MRI and histopathology in patients undergoing epilepsy surgery. Journal of neuroscience methods. 2012 Mar 30;205(1):182-9.

28. Ruifrok AC, Johnston DA. Quantification of histochemical staining by color deconvolution. Analytical and quantitative cytology and histology/the International Academy of Cytology [and] American Society of Cytology. 2001;23(4):291-9.

29. Soille P. Morphological image analysis: principles and applications: Springer-Verlag New York, Inc.; 2003.

30. Yushkevich PA, Piven J, Hazlett HC, et al. User-guided 3D active contour segmentation of anatomical structures: significantly improved efficiency and reliability. Neuroimage. 2006 Jul 1;31(3):1116-28.

31. Duvernoy HM CE, NaidichT, Fatterpekar GM, Raybaud C, Risold PY, Sakvolini U, Scarabino T. The human hippocampus: functional anatomy, vascularization and serial sections with MRI. 3rd Edition ed. Berlin Heidelberg: Springer Verlag; 2005.

32. Goubran M, Crukley C, de Ribaupierre S, Peters TM, Khan AR. Image registration of< i> ex-vivo</i> MRI to sparsely sectioned histology of hippocampal and neocortical temporal lobe specimens. NeuroImage. 2013;83:770-81.

33. Goubran M, de Ribaupierre S, Hammond RR, et al. Registration of in-vivo to ex-vivo MRI of surgically resected specimens: A pipeline for histology to in-vivo registration. Journal of neuroscience methods. 2014.

34. Gibson E, Gómez JA, Moussa M, et al., editors. 3D reconstruction of prostate histology based on quantified tissue cutting and deformation parameters. SPIE Medical Imaging; 2012: International Society for Optics and Photonics.

35. Goubran M, Rudko DA, Santyr B, et al. In vivo normative atlas of the hippocampal subfields using multi-echo susceptibility imaging at 7 Tesla. Human brain mapping. 2013;35:3588–601.

36. Goubran M, Hammond RR, de Ribaupierre S, et al. MRI and histology correlation in the neocortex of temporal lobe epilepsy. Annals of neurology. 2014.

37. Groppe DM, Urbach TP, Kutas M. Mass univariate analysis of event-related brain potentials/fields I: A critical tutorial review. Psychophysiology. 2011;48(12):1711-25.

38. Rugg-Gunn FJ, Eriksson SH, Symms MR, et al. Diffusion tensor imaging in refractory epilepsy. The Lancet. 2002;359(9319):1748-51.

39. Focke NK, Yogarajah M, Bonelli SB, Bartlett PA, Symms MR, Duncan JS. Voxel-based diffusion tensor imaging in patients with mesial temporal lobe epilepsy and hippocampal sclerosis. Neuroimage. 2008;40(2):728-37.

40. Thivard L, Lehéricy S, Krainik A, et al. Diffusion tensor imaging in medial temporal lobe epilepsy with hippocampal sclerosis. Neuroimage. 2005;28(3):682-90.

41. Khan AR, Goubran M, de Ribaupierre S, et al. Quantitative relaxometry and diffusion MRI for lateralization in MTS and non-MTS temporal lobe epilepsy. Epilepsy research. 2014;108(3):506-16.

42. Cantor-Rivera D, Khan AR, Goubran M, Mirsattari SM, Peters TM. Detection of Temporal Lobe Epilepsy using Support Vector Machines in Multi-parametric Quantitative MR Imaging. Computerized Medical Imaging and Graphics. 2014.

43. Kinoshita M, Hashimoto N, Goto T, et al. Fractional anisotropy and tumor cell density of the tumor core show positive correlation in diffusion tensor magnetic resonance imaging of malignant brain tumors. Neuroimage. 2008;43(1):29-35.

44. Coras R, Milesi G, Zucca I, et al. 7T MRI features in control human hippocampus and hippocampal sclerosis: An ex vivo study with histologic correlations. Epilepsia. 2014;55(12):2003-16.

45. Schmierer K, Parkes HG, So P-W, et al. High field (9.4 Tesla) magnetic resonance imaging of cortical grey matter lesions in multiple sclerosis. Brain : a journal of neurology. 2010;133(3):858-67.

46. Jurcoane A, Wagner M, Schmidt C, et al. Within-lesion differences in quantitative MRI parameters predict contrast enhancement in multiple sclerosis. Journal of Magnetic Resonance Imaging. 2013;38(6):1454-61.

47. Howell GA, Welch MG, Frederickson CJ. Stimulation-induced uptake and release of zinc in hippocampal slices. 1984.

48. Jardim AP, Neves RSdC, Caboclo LOSF, et al. Temporal lobe epilepsy with mesial temporal sclerosis: hippocampal neuronal loss as a predictor of surgical outcome. Arquivos de neuro-psiquiatria. 2012;70(5):319-24.

49. Pauli E, Hildebrandt M, Romstöck J, Stefan H, Blümcke I. Deficient memory acquisition in temporal lobe epilepsy is predicted by hippocampal granule cell loss. Neurology. 2006;67(8):1383-9.

50. Fuerst D, Shah J, Kupsky W, et al. Volumetric MRI, pathological, and neuropsychological progression in hippocampal sclerosis. Neurology. 2001;57(2):184-8.

Figure Legends

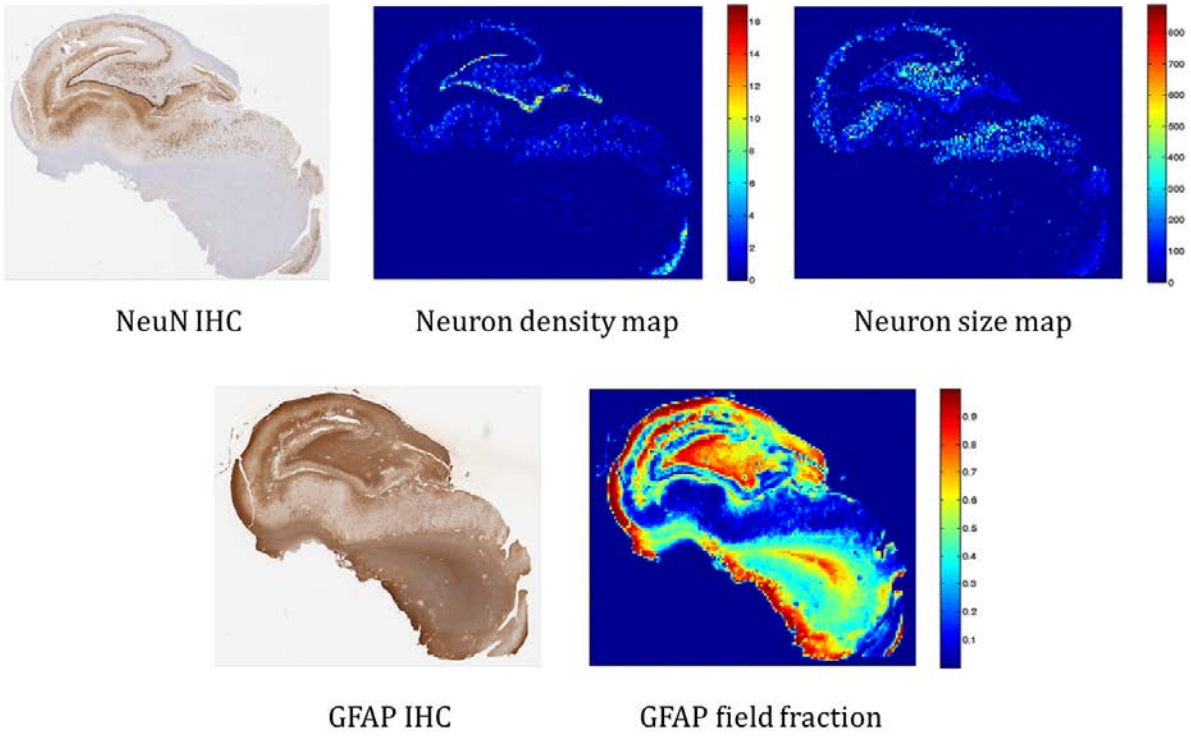

Figure 1. Overview of some of the quantitative histological features including: neuron density, mean neuron size, and GFAP field fraction.

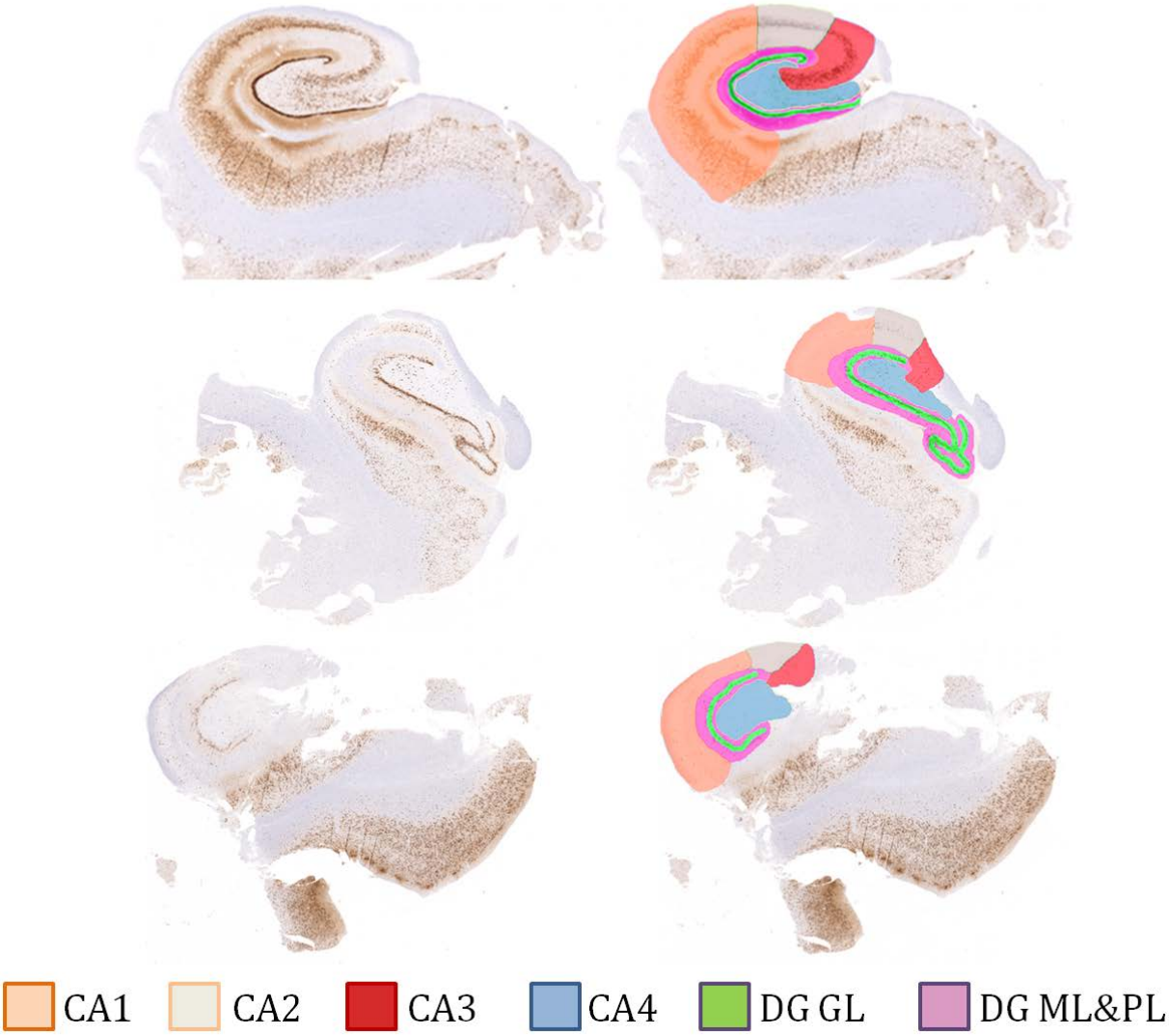

Figure 2. Subfield delineation on histology slices from three patients from our cohort (Top: Mild sclerosis, Middle: Moderate sclerosis, Bottom: Severe sclerosis). The labeling scheme (colour representing each subfield) is described at the bottom of the figure.

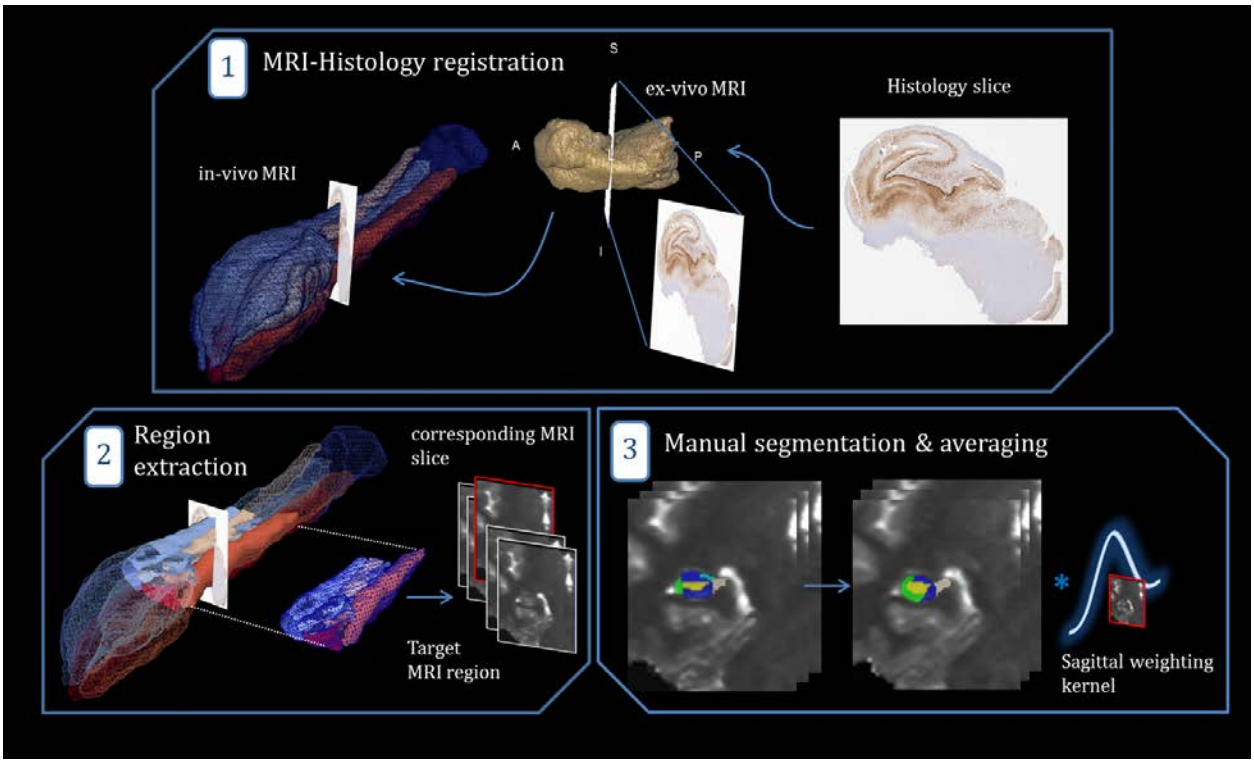

Figure 3. Schematic outline of MRI parameter extraction in the subfields. 1) Determination of the MRI slice best corresponding to a histology cut by employing a MRI-histology co-registration pipeline (with the ex-vivo MRI as an intermediate step). 2) Extraction of a subject-specific, target region surrounding the 'corresponding MRI slice', to model registration and sectioning uncertainty. 3) Manual delineation of the subfields within the chosen target region and application of a sinc sagittal weighting kernel (producing lower weighting away from the corresponding slice).

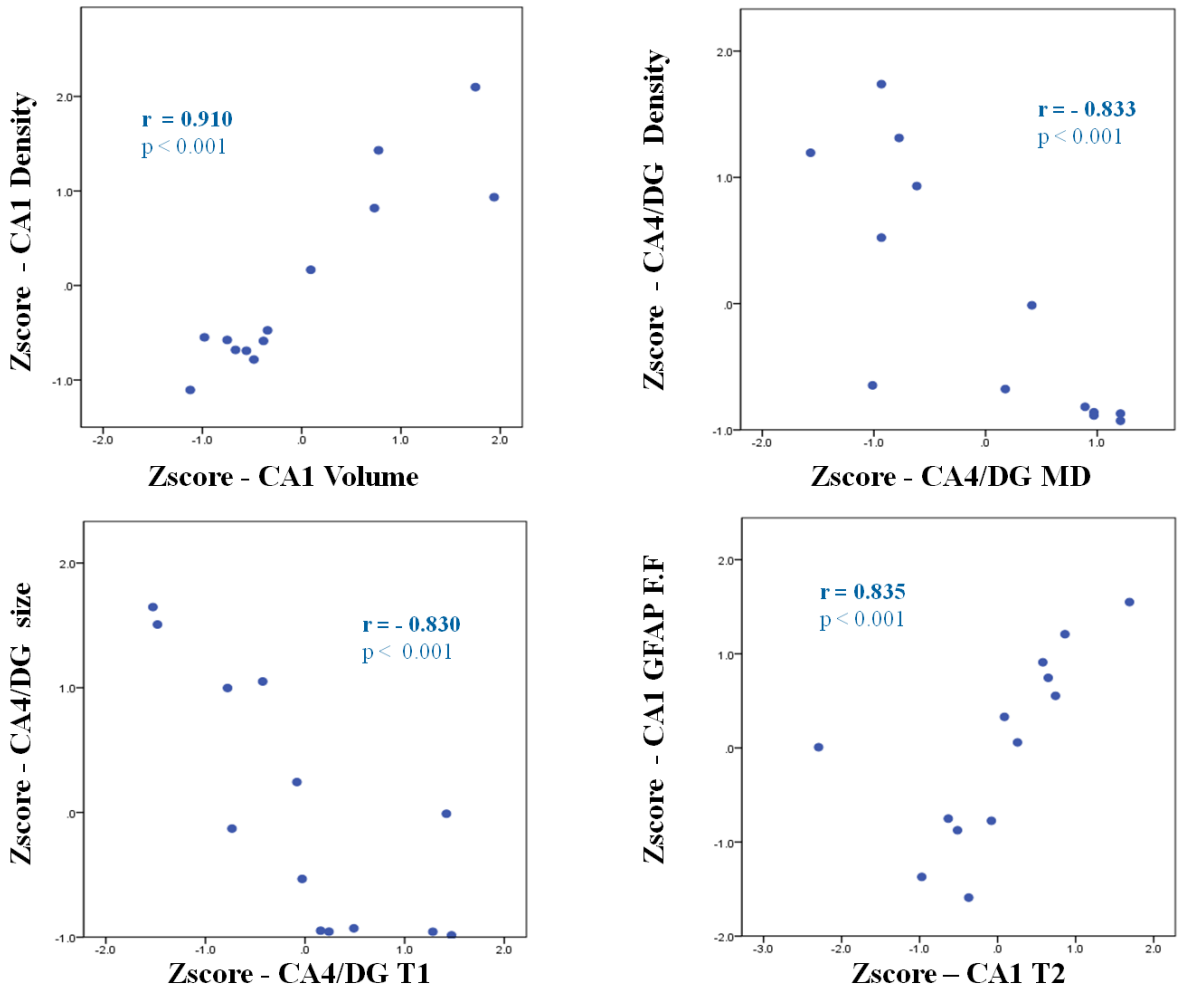

Figure 4. Selection of significant associations from Spearman's correlation analysis for subfield-specific MRI parameters with histological features.

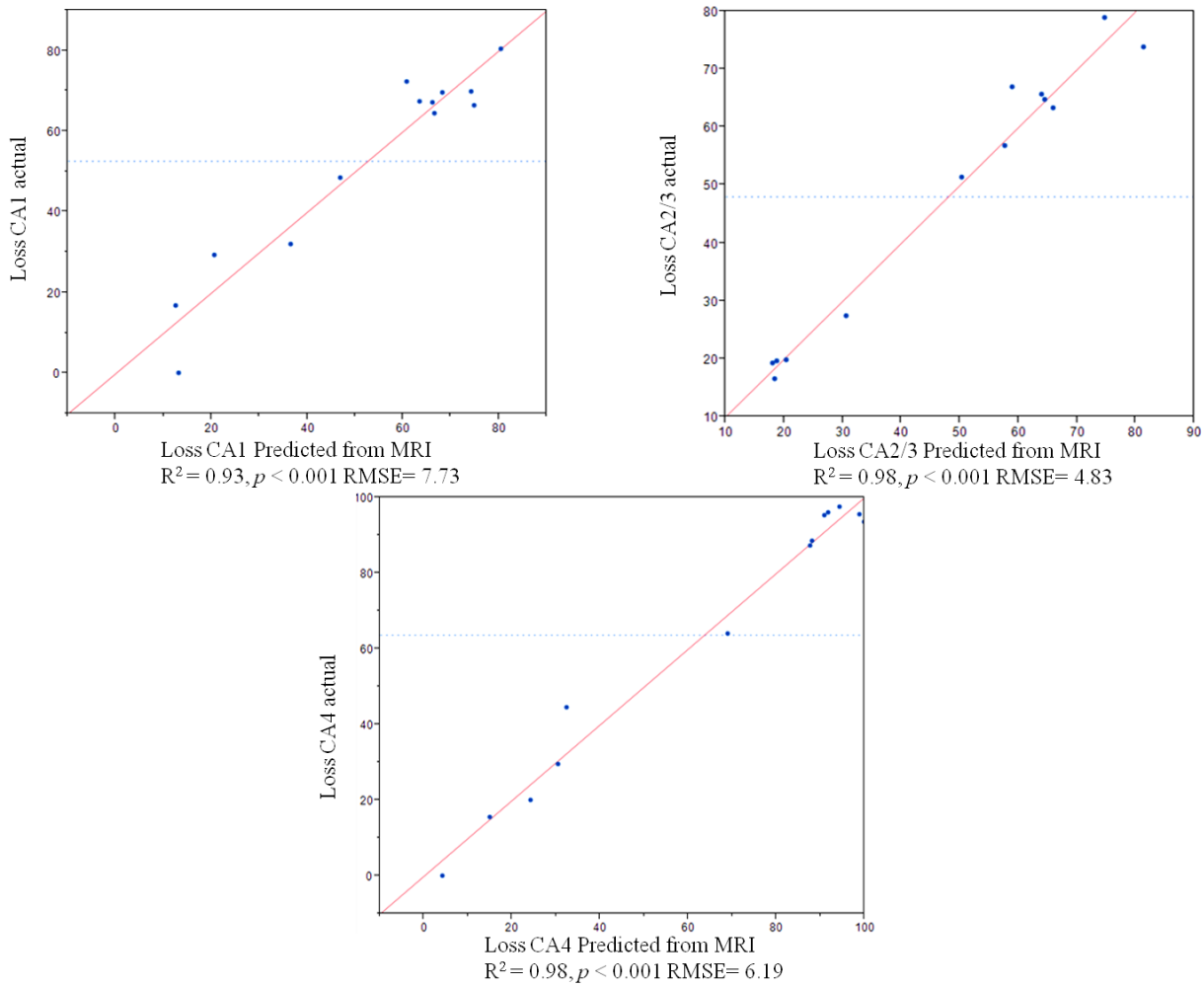

Figure 5. Multiple linear regression results for subfield-specific parameters depicting predicted vs. actual percent neuron loss for each of the four CA subfields.

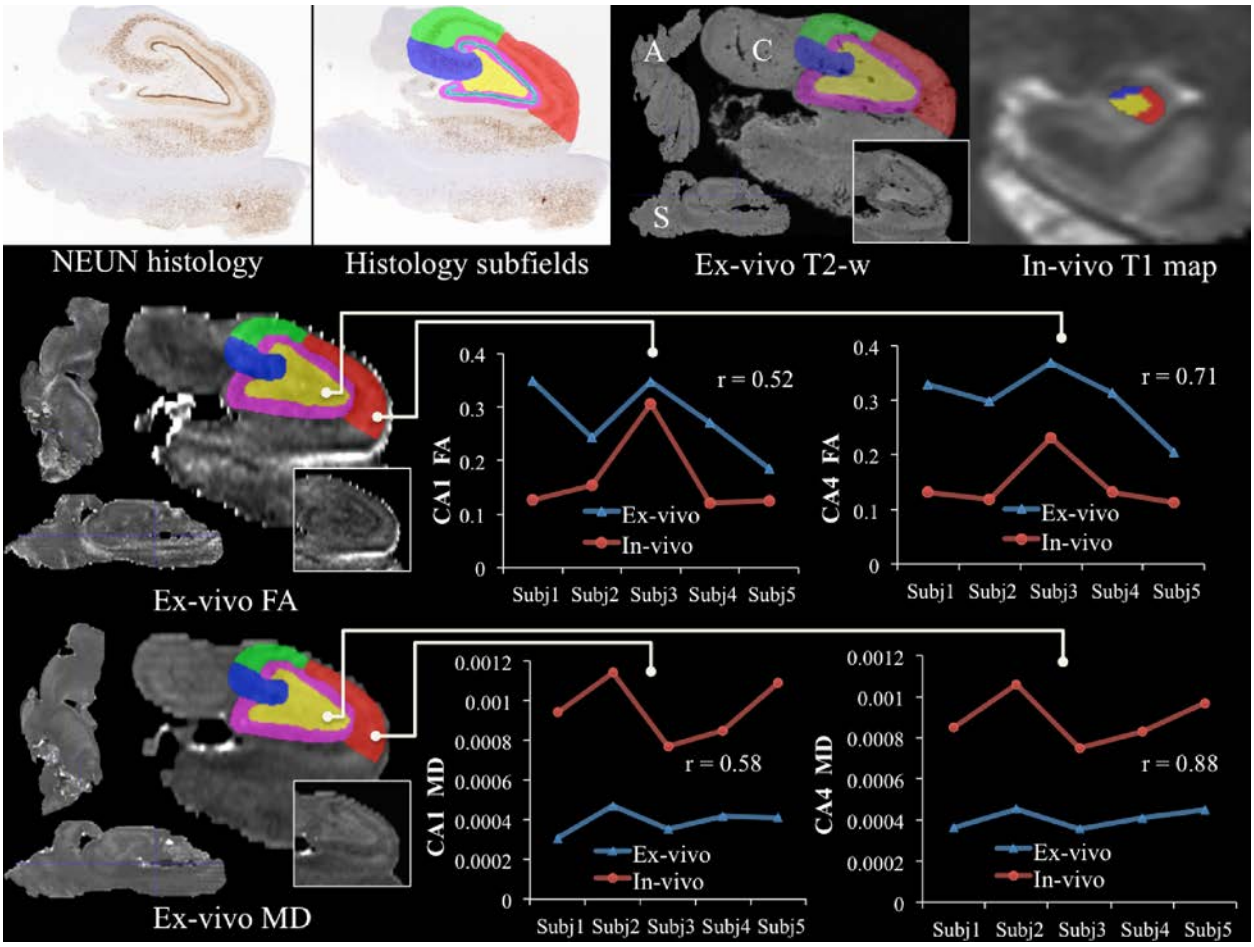

Figure 6. High-resolution *ex-vivo* validation of *in-vivo* DTI measurements. The top row depicts warping of the subfields from histology to the registered *ex-vivo* space for one subject and compares them to the *in-vivo* subfield segmentation (A: Axial, S: Sagittal, C: Coronal). Rows two and three demonstrate the comparison between *in-vivo* and *ex-vivo* DTI parameters [fractional anisotropy (FA) (middle row) and mean diffusivity (MD) (bottom row)] for both CA1 (middle) and CA4 (right).